Numerical modelling of shear localization in granular bodies using MPM and non-local hypoplasticity

Cite as: AIP Conference Proceedings **2239**, 020023 (2020); https://doi.org/10.1063/5.0007829
Published Online: 22 May 2020

Jakub Krzyżanowski, Michał Wójcik, and Jacek Tejchman

Numerical Modelling of Shear Localization in Granular Bodies using MPM and Non-local Hypoplasticity

Jakub Krzyżanowski[1,a)], Michał Wójcik[1,b)], and Jacek Tejchman[1,c)]

[1]*Gdansk University of Technology, Faculty of Civil and Environmental Engineering, Poland*

[a)]jakkrzy2@student.pg.edu.pl
[b)]michal.wojcik@pg.edu.pl
[c)]tejchmk@pg.edu.pl

Abstract. The paper deals with modelling of shear localization in granular bodies by means of an enhanced hypoplastic constitutive model and material point method (MPM). The calculations were carried out for plane strain compression of non-cohesive sand. In order to properly capture the width and inclination of shear zones, the constitutive model was enriched by a characteristic length of micro-structure by means of a non-local theory. The approach offered a good correspondence between numerical results and experimental ones.

INTRODUCTION

The material point method (MPM) [1] is a numerical technique for simulations of static and dynamic problems when large deformation occurs. Unlike the classical FEM, MPM is not bound to a deforming grid. MPM discretizes the fluid or solid body with a collection of material points. In each computational step, the information from those points is transferred to a background computational grid, which is usually fixed and where the governing equations are solved. The decoupling between material points and grid allows for avoiding the extensive mesh distortion and entanglement. For each time increment, the calculations within MPM include two steps: 1) a Lagrangian step and 2) a convective one. In the step '1', the computational mesh deforms together with the considered material. The state variables are calculated for each material point by the use of conventional shape functions and nodal parameters defined on the computational mesh. In the step '2', the convective step consists of mapping of the velocity field from material points to the computational grid that can remain at the same position as defined at the beginning of the time increment. The important differences with the conventional FEM are: a) the mass matrix varies with time, b) the gradient, stress and strain are evaluated at material points that can move from one element to another and c) the point masses appear in expressions for internal and external force vectors. The first MPM algorithm dated 1994 received many updates. The developments include explicit approaches. e. g. the Generalized Interpolation Material Point Method (GIMP) [2], Dual Domain Material Point Method (DDMP) [3], Convected Particles Domain Interpolation (CPDI) [4], [5]. There are also some implicit schemes [6], [7].

The intention of the current paper is to show some numerical results of shear localization in non-cohesive sand during plane strain compression with a hypoplastic constitutive law [8]-[10] based on MPM in the open-source software [11]. MPM is a dynamic explicit time integration approach. The Courant-Friedrichs-Lewy condition was used to determine a critical time step in numerical analyses. The paper consists of two parts. In the first part, some results of standard quasi-static geotechnical element tests with dry cohesionless sand (oedometric, triaxial compression and shear) using local hypoplasticity were shown. In the second part, the results of plane strain compression with a non-local hypoplastic model were described. The numerical results of quasi-static plane strain compression were compared to the corresponding experimental results with respect to the stress-strain evolution and geometry of shear zones.

4th Polish Congress of Mechanics and the 23rd International Conference on Computer Methods in Mechanics
AIP Conf. Proc. 2239, 020023-1–020023-11; https://doi.org/10.1063/5.0007829
Published by AIP Publishing. 978-0-7354-1998-8/$30.00

HYPOPLASTIC CONSTITUTIVE MODEL

Despite the discrete nature of granular materials, the mechanical behaviour of confined configurations in the quasi-static regime can be reasonably described by principles of continuum mechanics. Hypoplastic constitutive models were developed at Karlsruhe University [8]-[10]. The stress rate tensor is assumed to depend on stress, rate of deformation and void ratio via isotropic non-linear tensorial functions based on the representation theorem. The constitutive models were formulated by a heuristic process considering the essential mechanical properties of granular materials undergoing homogeneous deformation. A striking feature of hypoplasticity is that the constitutive equation is incrementally non-linear in deformation rate. The hypoplastic models are capable of describing some salient properties of granular materials, e.g. non-linear stress-strain relationship, dilatant and contractant volumetric change, stress level dependence, void ratio dependence, deformation direction dependence and strain softening. A further feature of hypoplastic models is the inclusion of the critical states, i.e. states in which a grain aggregate can deform continuously at constant stress and volume (void ratio). Moreover, both the coaxiality (coincidence of the direction of the principal stresses and principal plastic strain increments) and stress-dilatancy rule are not assumed a priori [12]. In contrast to some conventional elasto-plastic models, a decomposition of deformation into elastic and plastic parts, the formulation of a yield surface, plastic potential, flow rule and hardening rule are not needed. In spite of the fact that the failure surface and flow rule are not prescribed in hypoplasticity, they emerge as by-products [13]. The hallmarks of these models are their simple formulation and procedure for determining material parameters with standard laboratory experiments. The material parameters can be related to the granulometric properties of granular materials, such as grain size distribution curve, shape, angularity and hardness of grains [14]. A further advantage lies in the fact that one single set of material parameters is valid for a wide range of pressures and densities. The hypoplastic models describe the behaviour of so-called simple grain skeletons which are characterised by the following properties:

- the state is fully defined through the skeleton pressure and the void ratio (inherent anisotropy of contact forces between grains is not considered and vanishing principal stresses are not allowed),
- deformation of the skeleton is due to grain rearrangements (e.g. small deformation $<10^{-5}$ due to an elastic behaviour of grain contacts are negligible),
- grains are permanent (abrasion and crushing are excluded in order to keep the granulometric properties unchanged),
- three various void ratios decreasing exponentially with the pressure are distinguished (minimum, maximum and critical),
- the material manifests an asymptotic behaviour for monotonous and cyclic shearing or SOM-states for proportional compression,
- rate effects are negligible,
- physico-chemical effects (capillary and osmotic pressure) and cementation of grain contacts are not taken into account.

The summary of a local hypoplastic constitutive law for granular materials is given in Appendix (Eqs.A1-A10). The changes of the values of e_i, e_d and e_c decrease with the pressure σ_{kk} according to the exponential functions (Eq.A10) [9]. The general form of the constitutive model requires the following eight material parameters: e_{i0}, e_{d0}, e_{c0}, φ_c, h_s, β, n and α. The calibration procedure for the non-polar model and the material parameters for different sands was given by Bauer [9] and Herle and Gudehus [14]. The granulate hardness h_s and exponent n can be estimated from a single oedometric compression experiment with an initially loose specimen (h_s reflects the slope of the curve in a semi-logarithmic representation and n its curvature). The parameters α and β can be determined from a triaxial or plane strain test with an initially dense specimen (they reflect the height and position of the peak value of the stress-strain curve). The critical (residual) friction angle φ_c can be obtained from the angle of repose or measured in a triaxial test with a loose specimen. The parameters of e_{i0}, e_{d0} and e_{c0} are determined from conventional index tests ($e_{c0} \approx e_{max}$, $e_{d0} \approx e_{min}$, $e_{i0} \approx (1.1\text{-}1.5) e_{max}$). All parameters are valid for a pressure range of 1 kPa$<p_s<$1000 kPa. Below the stress level of 1 kPa, additional capillary forces due to the air humidity and van der Walls forces may become important. Above the stress level of 1000 kPa, grain crushing is expected. The MPM simulations were carried out with the following material constants for so-called Karlsruhe sand (mean grain diameter d_{50}=0.5 mm) which was used in experiments: e_{i0}=1.3, e_{d0}=0.51, e_{c0}=0.82, φ_c=30°, h_s=190 MPa, β=1, n=0.5 and α=0.3 [8], [9].

NON-LOCAL APPROACH

Hypoplastic constitutive models without a characteristic length can describe realistically the onset of shear localization but not its further evolution. An enhancement of the underlying constitutive model via a characteristic length is necessary for problems involving shear localization to regularize boundary value problems, to achieve objective and property convergent numerical solutions (mesh-independent load-displacement diagram and deformation patterns) [15]-[17].

A non-local approach was proposed forconcrete [18] and for soils [19] to regularize a boundary value problem and to calculate strain localization in the form of shear zones and cracks. It is based on spatial averaging of tensor or scalar state variables in a certain neighbourhood of a given point, i.e. material response at a point depends both on the state of its neighbourhood and on the state in the point itself. Thus, a characteristic length can be incorporated and softening can spread over material points. In contrast, in classical continuum mechanics, the principle of local action holds (i.e. the dependent variables in each material point depend only upon the values of the independent variables at the same point). To obtain a full regularisation effect according to both the mesh size and mesh inclination, it is sufficient to treat non-locally only one internal constitutive variable, e.g. equivalent plastic strain in elasto-plastic formulations [18], [19] or norm of the deformation rate in hypoplastic approaches [20], [21] whereas the other variables retain their local definitions. The advantages of a non-local approach are: it is suitable for both shear and tension dominated applications and is quite easy to implement in existing commercial codes. The disadvantages are: long computation time and the characteristic length is not directly related to micro-structure of materials (as e.g. in micro-polar hypoplasticity) [22]. The norm of the deformation rate expressed by $d=\|D_s\|$ was treated non-locally:

$$d^*(\boldsymbol{x}) = \frac{\int_V \omega(\|\mathbf{x}-\boldsymbol{\xi}\|)d(\boldsymbol{\xi})\mathrm{d}\boldsymbol{\xi}}{\int_V \omega(\|\mathbf{x}-\boldsymbol{\xi}\|)\mathrm{d}\boldsymbol{\xi}}\,, \tag{1}$$

where d^* - the non-local norm of deformation rate (Eq.A1), V - the body volume, $\mathbf{x}$ - the coordinates of the considered current point, $\boldsymbol{\xi}$ - the coordinates of the surrounding points and ω - the weighting function. Equation (1) does not alter a uniform field which means that it satisfies the normalizing condition [23]. As a weighting function ω, a Gauss distribution function was used [23]:

$$\omega(x) = \frac{1}{l_c\sqrt{\pi}}e^{-(r/l_c)^2}, \tag{2}$$

wherein the parameter l_c is the characteristic length of micro-structure and r is the distance between two points. The parameter l_c determines the size of the neighbourhood influencing the state at a given point. Generally, it is not directly related to dimensions of the material micro-structure since it depends on the constitutive model and the weighting function [22]. It is usually determined with an inverse identification process of experimental data [21] since itcannot be directly measured. The averaging in Eq.2 is restricted to a small representative area around each material point (the influence of points at the distance of $r=3l_c$ is only of 0.01%). For Karlsruhe sand, the characteristic length is about 1.5 mm ($3\times d_{50}$) [20]-[22].

ELEMENT TESTS

The results of 3 different usual geotechnical element tests were presented using a local hypoplastic law within MPM (oedometric compression, triaxial compression and shear with free dilatancy). The MPM schemes of tests were shown in Fig.1. Figure 2 presents the results of the evolution of the vertical normal stress σ_{11} versus the vertical normal strain ε_{11} for the different initial void ratio e_o and the evolution of void ratio e versus σ_{11}. The results of triaxial compression element tests with the constant lateral pressure σ_c for a freely moving smooth top boundary are demonstrated in Figs.3 and 4 (the evolution of the vertical normal stress σ_{11} versus the vertical normal strain ε_{11} for the different initial void ratio e_o, evolution of mobilized internal friction angle φ and void ratio e versus ε_{11} for the different initial void ratio e_o and σ_c). Finally, Fig.5 describes the evolution φ for the different e_o and normal pressure σ_n) for shear with free dilatancy, where the smooth top boundary could freely move in a vertical direction. All results of element tests are in agreement with experiments [8]-[10].

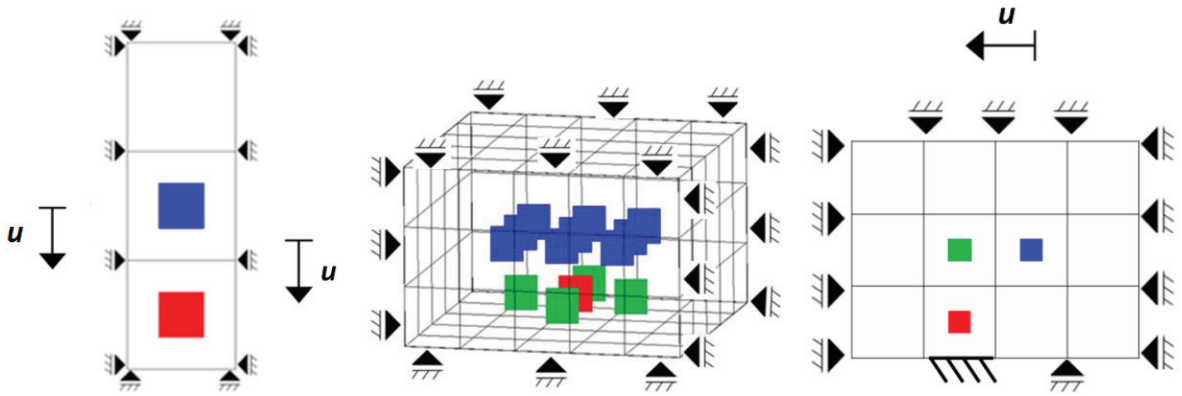

FIGURE 1. MPM mesh for element tests with boundary conditions: a) oedometric compression, b) triaxial compression and c) shear with free dilatancy (red colour - sand material, blue colour - rigid point, green colour - pressure point, u - rigid point displacement (corresponds to the displacement of the upper edge of the sample))

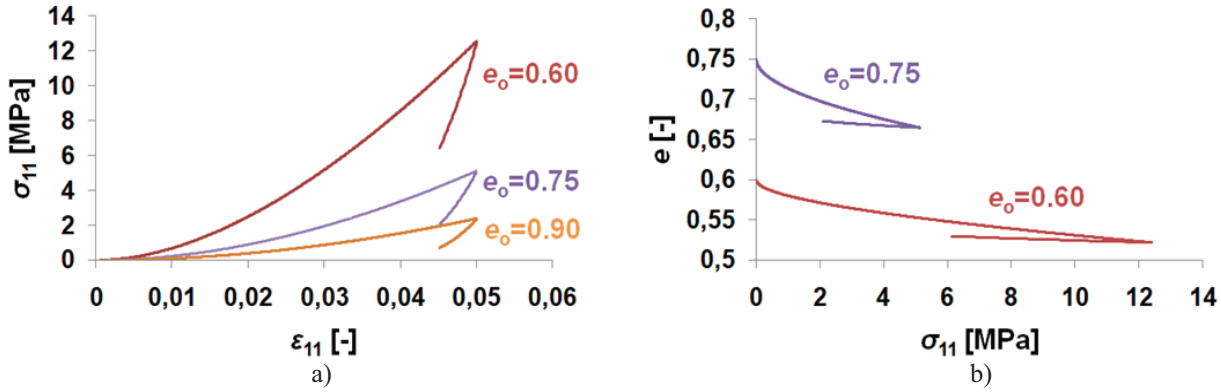

FIGURE 2. Oedometric compression element tests within MPM: (a) vertical stress σ_{11} versus vertical strain ε_{11}, (b) void ratio e versus vertical stress σ_{11}

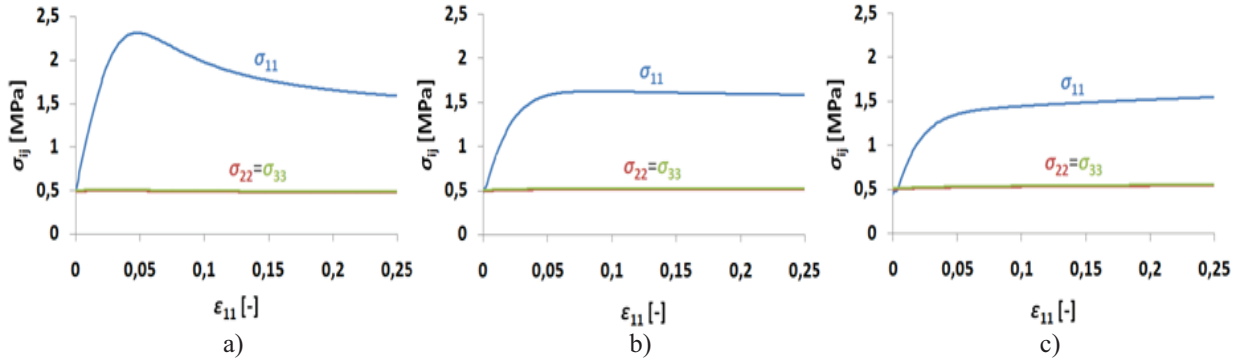

FIGURE 3. Evolution of stresses σ_{ij} versus vertical strain ε_{11} during triaxial compression element tests within MPM for lateral pressure σ_c=0.5 MPa and different initial void ratios of sand: a) e_o=0.60, b) e_o=0.75 and c) e_o=0.90

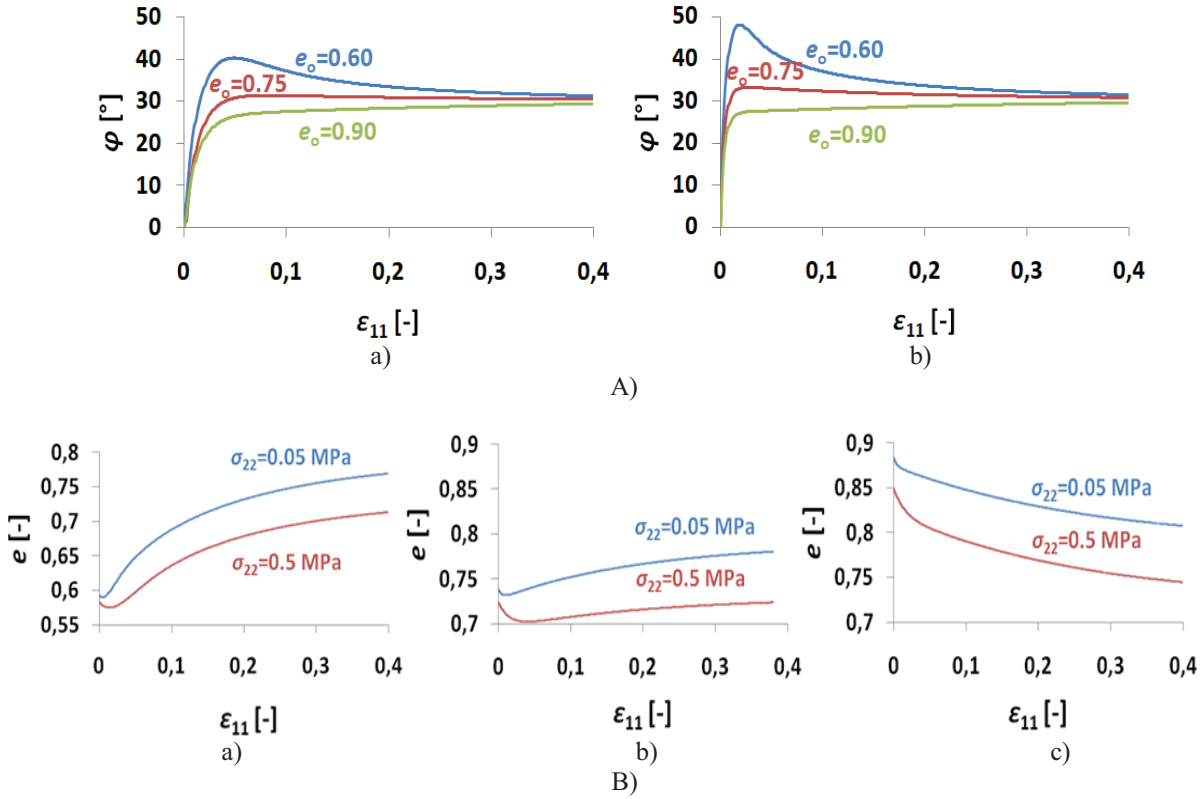

FIGURE 4. Evolution of mobilized internal friction angle φ A) and void ratio e B) versus vertical strain ε_{11} during triaxial compression element tests for different initial void ratios of sand: a) e_o=0.60, b) e_o=0.75, c) e_o=0.90 and lateral pressure: a) σ_c=500 kPa, and b) σ_c=50 kPa

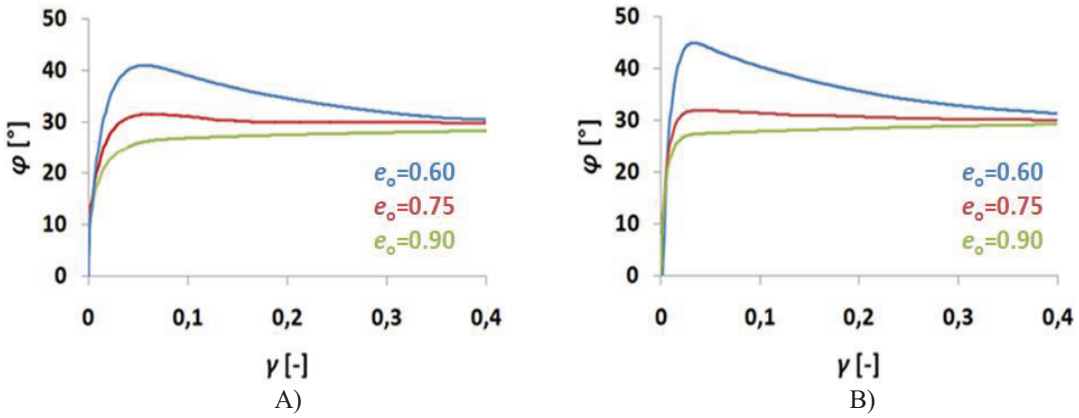

FIGURE 5. Evolution of mobilized internal friction angle φ versus shear strain γ during simple shear element test with free dilatancy for different initial void ratio of sand: a) e_o=0.60, b) e_o=0.75 and c) e_o=0.90 and normal pressures: A) σ_n=200 kPa and B) σ_n=50 kPa

PLANE STRAIN COMPRESSION

The sand specimen with the size of 140×40 mm^2 ($h_o \times b_o$) (as in the experiment [24]) was numerically simulated under plane strain conditions. The uniform vertical displacement was prescribed along the smooth top boundary to enforce compressive deformation. The horizontal displacements along horizontal boundaries were free. To preserve the specimen stability, the mid-point along the smooth specimen bottom was kept fixed. Quadrilateral finite elements for background mesh were used (Fig.6) with one material point in the element. Gravity was taken into

account. To induce a shear zone, a single imperfection of the element size 5×5 mm^2 with a higher initial void ratio (e_o=0.90) was inserted at the specimen mid-height.

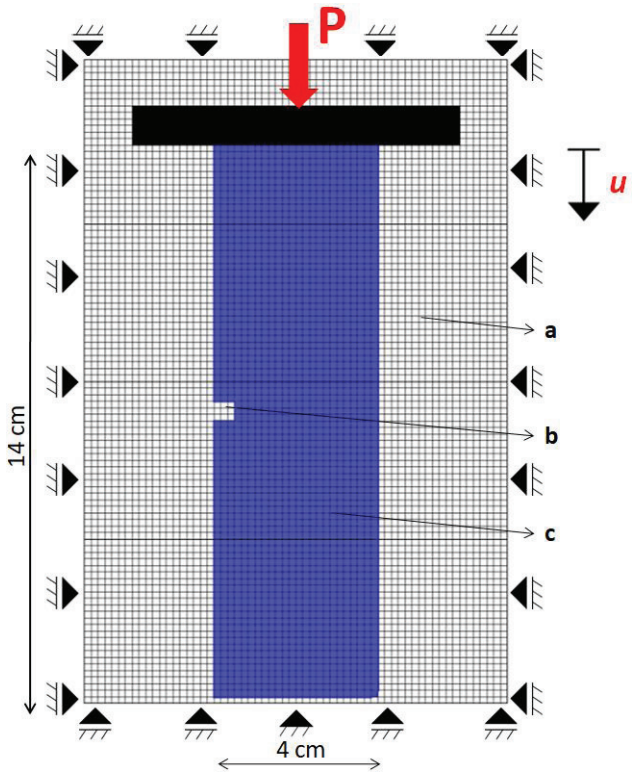

FIGURE 6. Boundary conditions, specimen geometry and computational MPM mesh during plane strain compression test (P - vertical top force, u - vertical top edge displacement, a) computational mesh, b) imperfection and c) specimen)

The MPM calculations were performed with the different time steps Δt=5×10^{-8}-5×10^{-6} s and different material point meshes: 16×56, 24×84 and 32×112. The meshes corresponded to the element size 2.5×2.5 mm^2, 1.66×1.66 mm^2 and 1.25×1.25 mm^2, respectively. The evolution of the mobilized internal friction angle φ against the vertical strain u/h_o is shown in Fig.7 for different time steps and three different numbers of material points (p=50 kPa, e_o=0.55 and l_c=1.5 mm). The optimum time increment was found to be Δt=1×10^{-7} for the mesh composed of 24×84 points (finite element size was 1.66×1.66 mm^2). No mesh dependence occurred.

The effect of the characteristic length l_c is shown in Fig.8. The characteristic lengths ranged from l_c=0 mm up to l_c=4 mm. The initial void ratio was set as e_o=0.55 and the lateral pressure as p=50 kPa. Similarly as in the real experiments [24], the initially dense specimen showed an asymptotic behaviour; it exhibited initially small elasticity, hardening, reached a peak strength, gradually softened and dilated reaching a residual state (Fig.8A).The maximum internal friction angles ϕ^{peak} and residual internal friction angle ϕ_{res} increased with growing l_c. For l_c=1.5 mm, the internal friction angles were: ϕ^{peak}=55^{o}for u/h_o=1.2% and ϕ_{res}=30^o for u/h_o=4.0%.

During deformation, a distinct internal inclined shear zone occurred inside the sand specimen which was marked by shear strain and volume increase (Fig.8B). During deformation, initially two shear zones occurred, starting from the initial imperfection. Later, a single shear dilatant zone dominated that started to propagate just before reaching the peak force. For l_c=1.5 mm, the final inclined shear zone developed in the upper part of the specimen, whereas for l_c>1.5 mm, it was located in the lower specimen part (Fig.8B).The thickness of the shear zone was determined by assuming e_o≥0.70. The thickness of the inclined dilatant shear zone grew with increasing l_c. It was on average in the residual state (for l_c=1.5 mm) about t_s=7.5 mm=5×l_c=15×d_{50} based on the dilatant region and its inclination against the bottom was about 55°. The critical void ratio was reached in the shear zone (Fig.9). Those outcomes are quantitatively in agreement with the experiment [24].

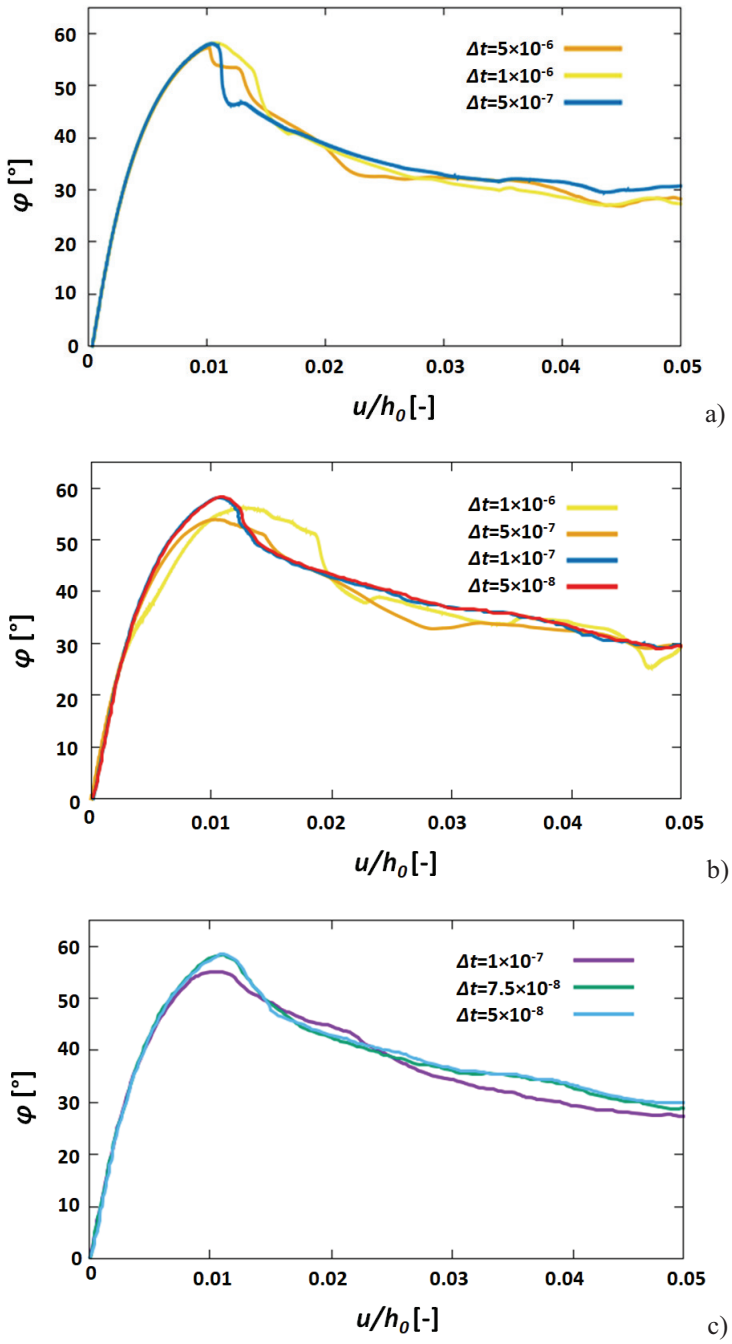

FIGURE 7. Numerical evolution of mobilized internal friction angle φ versus vertical strain u/h_o (p=50 kPa, e_o=0.55 and l_c=1.5 mm) for different material point meshes and time steps Δt: a) mesh 16×56 (element size 2.5×2.5 mm^2), b) mesh 24×84 (element size 1.66×1.66 mm^2) and c) mesh 32×112 (element size 1.25×1.25 mm^2)

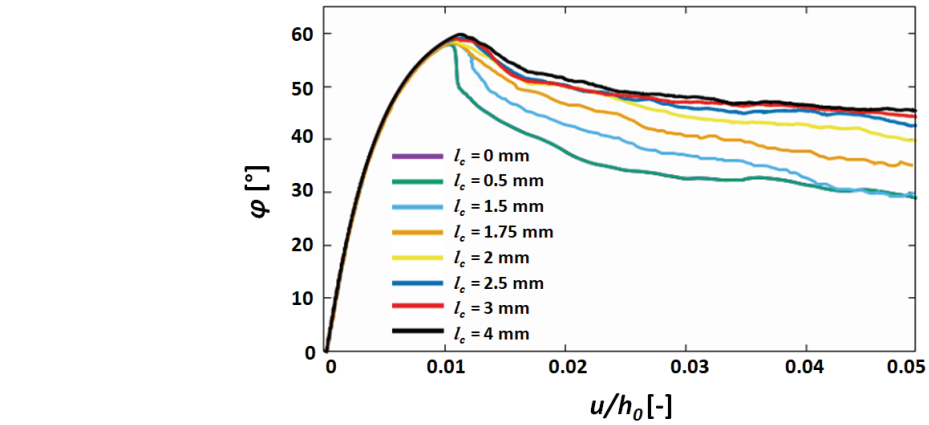

A)

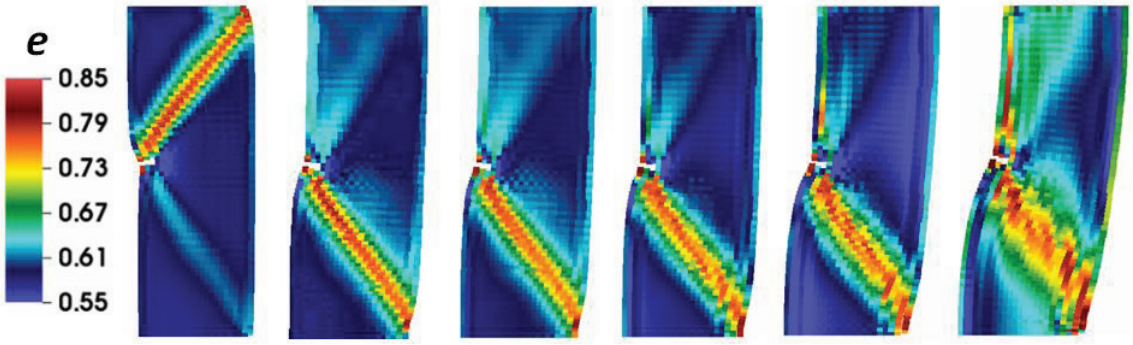

a) b) c) d) e) f)

B)

FIGURE 8. Evolution of mobilized internal friction angle ϕ versus vertical strain u/h_o(p=50 kPa and e_o=0.55) (A) and deformed specimens from numerical simulations for u/h_o=5.0% with distribution of void ratio e (B) for different characteristic lengths l_c=0-4 mm: a) l_c=1.5 mm, b) l_c=1.75 mm, c) l_c=2 mm, d) l_c=2.5 mm, e) l_c=3 mm and f) l_c=4 mm

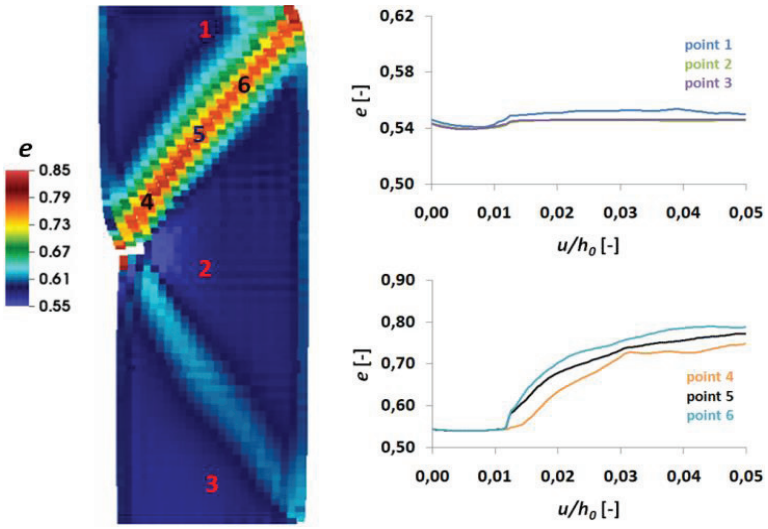

FIGURE 9. Evolution of void ratio e outside (points '1', '2' and '3') and inside shear zone (points '4', '5' and '6') versus vertical strain u/h_o for initially dense sand from numerical simulations (p=50 kPa, e_o=0.55 and l_c=1.5 mm)

Figure 10 describes the influence of the initial void ratio of sand e_o=0.55-0.90 on the mobilized internal friction angle and shear localization (p=50 kPa and l_c=1.5 mm). As the initial void ratio increased, the peak internal friction angle decreased: ϕ^{peak}=55° for e_o=0.55, ϕ^{peak}=40° for e_o=0.75 and ϕ^{peak}=30° for e_o=0.90. With increasing e_o up to $e_o \leq 0.75$ the thickness of the shear zone t_s increased: $t_s=5\times l_c$ for e_o=0.55 and $t_s=6\times l_c$ for e_o=0.75. No shear zone was observed for initially loose specimen (e_o=0.90). The inclination of the shear zone to the horizontal θ decreased with increasing e_o: θ=56° for e_o=0.55 and θ=50° for e_o=0.75.

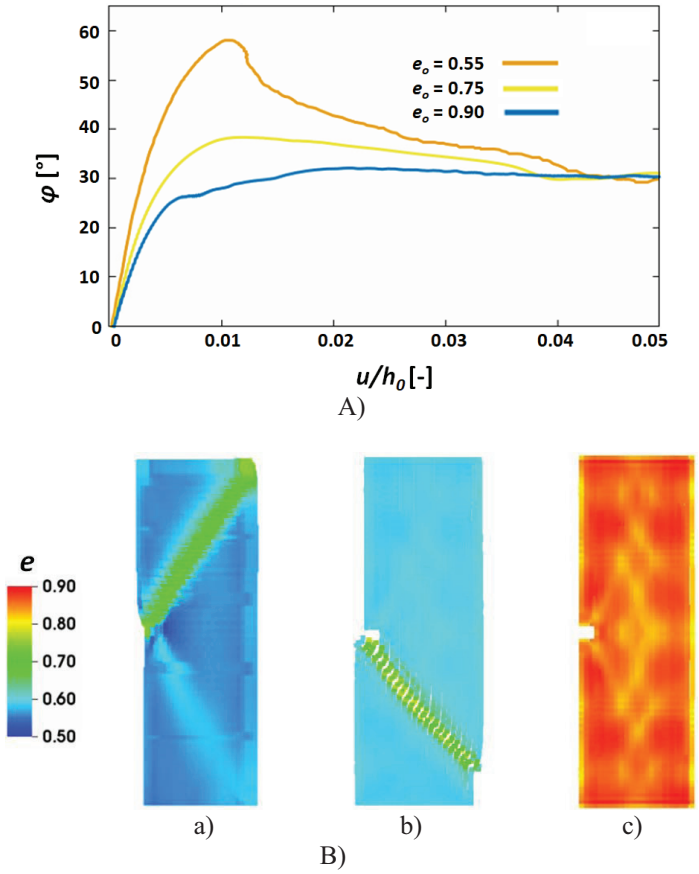

FIGURE 10. Evolution of mobilized internal friction angle ϕ versus vertical strain u/h_o (p=50 kPa, l_c=1.5 mm) and deformed specimens for u/h_o=5.0% with distribution of void ratio e for different initial void ratio: a) e_o=0.55, b) e_o=0.75 and c) e_o=0.90

CONCLUSIONS

MPM in contrast to standard Lagrangian approaches allows for simulating granular flow without excessive mesh distortion. MPM based on a non-local hypoplastic constitutive model realistically described shear localization in a granular body during plane strain compression. The numerical outcomes were insensitive of the number of material points and the time increment. The thickness of shear zones became greater with increasing characteristic length and initial void ratio. The granular material always manifested an asymptotic behaviour in the residual state by reaching a critical state.

APPENDIX

The hypoplastic model [8], [9] describes the evolution of normalized stress tensor $\hat{T}_s$ with the evolution of rate of deformation tensor D_s by isotropic linear and non-linear tensorial functions L and N (index 's' denotes the skeleton):

$$\mathring{\hat{T}}_s = f_s\left[L\left(\hat{T}_s, D_s\right) + f_d N\left(\hat{T}_s\right)\|D_s\|\right], \tag{A1}$$

where $\mathring{T}_s$ is the Jaumann stress rate tensor, f_s is the stiffness factor and f_d is the density factor. The normalized stress tensor is defined as follows:

$$\hat{T}_s = \frac{T_s}{trT_s}, \tag{A2}$$

where T_s is the Cauchy stress tensor. The following representations for L and N (which are linear and non-linear in D_s) are proposed:

$$L(\hat{T}_s, D_s) = a_1^2 D_s + \hat{T}_s tr(\hat{T}_s D_s), \tag{A3}$$

$$N(\hat{T}_s) = a_1(\hat{T}_s + \hat{T}_s^*), \tag{A4}$$

where

$$a_1^{-1} = c_1 + c_2\|\hat{T}_s^*\|[1 + cos(3\theta)], cos(3\theta) = -\sqrt{6}\frac{tr(\hat{T}_s^{*3})}{[tr(\hat{T}_s^2)]^{1.5}}, \tag{A5}$$

$$c_1 = \sqrt{\frac{3}{8}}\frac{(3-\sin\varphi_c)}{\sin\varphi_c}, c_2 = \frac{3}{8}\frac{(3+\sin\varphi_c)}{\sin\varphi_c}. \tag{A6}$$

Herein φ_c - critical angle of internal friction during stationary flow and θ-Lode angle. The $\hat{T}_s^*$ is the deviatoric part of the normalized stress tensor $\hat{T}_s$

$$\hat{T}_s^* = \hat{T}_s - \frac{1}{3}I. \tag{A7}$$

The influence of the current density and the pressure level is taken into account by the stiffness factor f_s (proportional to the granular hardness h_s and depending also on the mean stress and void ratio) and the density factor f_d which are represented as:

$$f_s = f_b f_e = \frac{h_s}{nh_i}\left(\frac{e_i}{e}\right)^{\beta}\frac{1+e_i}{e_i}\left(\frac{3p_s}{h_s}\right)^{1-n}, f_d = \left(\frac{e-e_d}{e_c-e_d}\right)^{\alpha}, \tag{A8}$$

where α - pycnotropy coefficient, n - compression coefficient, β - stiffness coefficient, a_1 - parameter representing the deviatoric part of the normalized stress in critical states, e_c - critical void ratio, e_d - void ratio at maximum densification, e_i - maximum void ratio. The current void ratio e is updated during calculations by the formula:

$$\dot{e} = (1 + e)trD, \tag{A9}$$

where $\dot{e}$ - rate of the void ratio (e is limited by e_i and e_d). The changes of the values of e_i, e_d and e_c decrease with the pressure p_s according to the exponential functions:

$$e_i = e_{i0} \cdot exp\left[-\left(\frac{-3p_s}{h_s}\right)^n\right], e_d = e_{d0} \cdot exp\left[-\left(\frac{-3p_s}{h_s}\right)^n\right], e_c = e_{c0} \cdot exp\left[-\left(\frac{-3p_s}{h_s}\right)^n\right], \tag{A10}$$

where e_{i0}, e_{d0}, e_{c0} are the values of e_i, e_d and e_c for the pressure p_s=0.

Acknowledgements

The research work has been carried out within the project "Autogeneous coupled dynamic-acoustic effects in granular materials - experiments and coupled DEM/CFD approach" financed by the National Research Centre, Poland (NCN) (UMO-2017/27/B/ST8/02306).

REFERENCES

1. Sulsky D., Chen Z., Schreyer HL (1994) A particle method for history-dependent materials. *Comput. Methods Appl. Mech. Engrg.* 118: 179-196.
2. BardenhagenSG., KoberEM. (2004) The Generalized Interpolation Material Point Method. *Comput. Model. Eng. & Sci.*5:477-495.
3. Zhang D., Ma X., Giguere P. (2011) Material Point Method enhanced by modified gradient of shape function. *J. Comput. Phys.*230: 6379-6398.
4. Sadeghirad A., Brannon R., Guilkey J. (2013) A convected particle domain interpolation technique to extend applicability of the material point method for problems involving massive deformations. *Int. J. Numer. Meth. Eng.*86: 1435-1456.
5. Sadeghirad A., Brannon R., Burghardt J. (2011) A convected particle domain interpolation technique to extend applicability of the material point method for problems involving massive deformations", *International Journal for numerical methods in Engineering*.86, 1435-1456.
6. Cummins SJ., Brackbill SU. (2002) An Implicit Particle-in-Cell Method for Granular Materials. *J. Comput. Phys.*180: 506-548.
7. Charlton TJ., Cooms WM., Augarde CE. (2017) iGIMP: An implicit generalized interpolation material point method for large deformations. *Comput. Struct.,* 190: 108-125.
8. Gudehus G. A. Comprehensive constitutive equation for granular materials. *Soils and Foundations* 36(1), 1-12, 1996.
9. Bauer E. (1996) Calibration of a comprehensive hypoplastic model for granular materials. *Soils and Foundations* 36(1), 13-26, 1996.
10. Von Wolffersdorff, P. A. A hypoplastic relation for granular materials with a predefined limit state surface. *Mechanics Cohesive-Frictional Materials* 1: 251-271, 1996.
11. Uintah Software. Utah University (USA), http://www.uintah.utah.edu.
12. Tejchman J. Wu W. FE-investigations of non-coaxiality and stress-dilatancy rule in dilatants granular bodies within micro-polar hypoplasticity. *Int. Journal for Numerical Analytical* Methods *in Geomechanics,*117-142, 2009.
13. W. Wu., A. Niemunis, Failure criterion, flow rule and dissipation function derived from hypoplasticity. *Mech. Cohes.-Frict. Mater.* 1 (1996), 145-163.
14. I. Herle, G. Gudehus, Determination of parameters of a hypoplastic constitutive model from properties of grain assemblies, *Mech. Cohes.-Frict. Mater.*, 4 (5) (1999) 461-486.
15. J. Tejchman, E. Bauer, FE-simulations of a direct and a true simple shear test within a polar hypoplasticity, *Computers and Geotechnics*32 (1) (2005)1-16.
16. J. Tejchman, W. Wu. Boundary effects on behaviour of granular material during plane strain compression. *European Journal of Mechanics / A Solids*,29 (2010) 18-27.
17. J. Tejchman, J. Górski, FE study of patterns of shear zones in granular bodies during plane strain compression. *ActaGeotechnica*5 (2) (2010) 95-112.
18. Z. P. Bazant, F. Lin, G. Pijaudier-Cabot, Yield limit degradation: non-local continuum model with local strain, in: Owen (Ed.), Proc. Int. Conf. Computational Plasticity, Barcelona, 1987, pp. 1757-1780.
19. Brinkgreve R., Geomaterial models and numerical analysis of softening. Dissertation, Delft University, 1-153, 1994.
20. Wójcik, M., Tejchman, J. Modelling of shear zone localization during confined granular flow in silos with non-local hypoplasticity. *Powder Technology* 192, 298-310, 2009.
21. Tejchman J., *FE modelling of shear localization in granular bodies with micro-polar hypoplasticity*, Springer Series in Geomechanics and Geoengineering, Berlin-Heidelberg, 2008.
22. Tejchman J., Influence of a characteristic length on shear zone formation in hypoplasticity with different enhancements. *Computers and Geotechnics* 31, 8, 595-611, 2004.
23. Z. Bazant, M. Jirasek, Nonlocal integral formulations of plasticity and damage: survey of progress. *Journal of Engineering Mechanics* 128, 11, 2002, 1119-1149.
24. Vardoulakis, I. Shear band inclination and shear modulus in biaxial tests. *International Journal for Numerical and Analytical Methods in Geomechanics*4, 103-119, 1980.